Martin, L.G. et al. (2013). Pt-Sn/C as a possible methanol-tolerant cathode catalyst for DMFC. Electrocatalysis, 4: 144 – 153.
http://dx.doi.org/10.1007/s12678-013-0131-8

Pt–Sn/C as a possible methanol-tolerant cathode catalyst for DMFC

Lynwill G. Martin, Ivan Green, X. Wang, Sivakumar Pasupathi and Bruno G. Pollet

Abstract

An effective method was developed for preparing highly dispersed nano-sized Pt–Sn/C electrocatalyst synthesised by a modified polyol reduction method. From XRD patterns, the Pt–Sn/C peaks shifted slightly to lower 2θ angles when compared with commercial Pt/C catalyst, suggesting that Sn formed alloy with Pt. Based on HR-TEM images, the Pt–Sn/C nanoparticles showed small particle sizes and well dispersed onto the carbon support with a narrow particle distribution. The methanol oxidation reaction on the as-prepared Pt–Sn/C catalyst appeared at lower currents (+7.08 mA at +480 mV vs. Ag/AgCl) compared to the commercial Pt/C (+8.25 mA at +480 mV vs. Ag/AgCl) suggesting that the Pt–Sn/C catalyst has 'methanol tolerance capabilities'. Pt–Sn/C HA Slurry pH3 catalysts showed better activity towards the oxygen-reduction reaction (ORR) than commercial Pt/C which could be attributed to smaller particle sizes. In our study, the Pt–Sn/C catalyst appears to be a promising methanol-tolerant catalyst with activity towards the ORR in the DMFC.

Introduction

In recent years, considerable attention and R&D funding have been injected into direct methanol fuel cell (DMFC) technologies. There are a large number of applications for DMFCs especially in stationary devices, portable electrical devices and transportation [1]. The use of methanol as a fuel has a few advantages in comparison to hydrogen. For example, methanol is an inexpensive liquid fuel which can be easily transported, stored and handled [1, 2]. However, despite these advantages and progress made in the development of DMFCs, the performance is still limited due to the poor kinetics of both anode and cathode reaction and the methanol crossover from the anode to the cathode side through the polymer electrolyte membrane (PEM) [3, 4]. In many cases, this methanol crossover issue decreases the fuel cell efficiency and produces mixed currents due to methanol oxidation on the cathode side, resulting in cell voltage losses [2–4]. Moreover, the crossover effect in the DMFC membrane causes a further decrease in the cathode efficiency due to the occurrence of a mixed potential, which results from the competitive reaction between oxygen reduction and methanol oxidation on Pt cathode [5]. To avoid this problem, one strategy is to modify the existing membranes or to develop novel membranes with less methanol permeability. Another approach is to develop methanol-tolerant cathode catalysts such as binary platinum alloys containing Co, Ni, Fe and Cr [5–7]. Various

transition-metal macrocycles [8–10] and ruthenium-based chalcogenides [11, 12] have also been tested as methanol-tolerant oxygen cathodes because these compounds are inactive toward the oxidation of methanol. However, the catalytic activities of these catalysts for the oxygen-reduction reaction (ORR) are still lower than those of Pt-based catalysts, and the long-term stability under fuel cell conditions at high potentials has not been well tested as compared to Pt-based catalysts [13]. Thus, it is necessary to develop novel Pt-based electrocatalysts, which can catalyse the oxygen reduction with limited oxidation of methanol.

Pt–Sn/C nanoparticles have been studied for decades as anode catalysts for the electro-oxidation of methanol and ethanol due to the fact that Sn enhances the catalytic activity of Pt towards alcohol oxidation [14]. Several research groups have studied this electrocatalyst, and inconsistencies in catalyst performance for alcohol oxidation have been reported. Although superior performances of Pt–Sn catalyst are widely reported in the literature, some studies show negligible or even no enhancements of the methanol oxidation reaction (MOR) rate over Pt catalyst [14–16]. The improvements of Pt–Sn were attributed to overriding effects namely the involving 'ensemble' effect rather than the addition of Sn for methanol oxidation [4, 17]. Studies performed by Colmati et al. [18] show that due to the alloying of Sn with Pt the adsorption/dehydrogenation of methanol becomes more difficult, and methanol oxidation only occurs at moderate alloying. Because of this interesting finding, it is of interest to investigate the possibility of using the Pt–Sn alloy system as a possible methanol-tolerant cathode catalyst. Only a few reports are available where the Pt–Sn/C system has been used as a cathode catalyst in DMFCs. Jeyabharathi et al. [19] reported that the as-prepared Pt–Sn/C catalyst shows mixed behaviour when compared to the catalyst subjected to heat treatment. The methanol tolerance increases with increased temperatures whereas the ORR activity remains the same. They also demonstrated that heat treatment of the catalysts have a significant effect on the ORR activity and the resistance of the Pt–Sn/C catalyst towards methanol. You et al. [20] also showed that Pt–antimony tin oxide nanoparticles can be used as cathode catalyst in DMFC, and Parrondo et al. reported that Pt–SnO_X cathode catalyst can be used in high-temperature PEM fuel cells [21].

Here in this study, we synthesised Pt–Sn/C nanoparticles via a modified polyol reduction process by sonicating the reaction mixture beforehand, adding carbon in different forms, refluxing the metals first, and adding HCl as sedimentation promoter in order to increase the metal loading and synthesise Pt–Sn nanoparticles with smaller sizes and narrower particle size distribution, and studying the effect of all these parameters on the ORR activity and methanol tolerance of Pt–Sn catalyst.

Experimental Methods

Materials

All chemicals used in this study were of analytical grade. $H_2PtCl_6{\cdot}6H_2O$, GR (Merck) and $SnCl_2{\cdot}2H_2O$, GR (Merck) were used as metal precursors. Vulcan XC-72R carbon black was used for supporting the produced metallic nanoparticles. Ethylene glycol (EG), GR (Merck) was

used as a solvent and a reducing agent. Twenty percent Pt/C HiSPEC™ 3000 (Alfa Aesar, Johnson Matthey) was used for comparison purposes. All solutions were prepared using ultrapure water (MilliQ, Millipore 18.2 MΩ).

Synthesis of Carbon Supported Pt–Sn Nanoparticles

Standard Method (STD)

Six Pt–Sn/C catalyst samples were prepared by a modified polyol reduction process under N_2 described as follows: To a mixture of H_2 $PtCl_6$ $\cdot 6H_2$ O, a calculated amount of $SnCl_2 \cdot 2H_2O$ and Vulcan XC-72R carbon was suspended in EG in a Schlenk tube. The pH value of the solution was increased to about 13 by using a 1 M NaOH solution followed by magnetic stirring and purging with N_2. The solution was then heated at 150 °C for 4 h and then set aside to cool to room temperature and stirred overnight. The catalyst was filtered and the filter cake thoroughly washed with ultrapure water and dried in a vacuum oven at 80 °C overnight. The nominal Pt loading was 20 wt.% and the nominal atomic ratio of Pt and Sn was 3:1. Several variations were performed on the standard polyol method described above.

Acid Method

After the reaction mixture was cooled down to room temperature, the pH of the colloidal suspension was adjusted to either 3 or 5 using 32 % HCl and then stirred overnight. Here, HCl acted as a sedimentation promoter which in turn improved the overall metal loading of the catalyst.

Slurry Method

In this method, the Vulcan X-72 was added as slurry. The carbon black powder was added to 10 ml EG and sonicated (ultrasonic bath, 40 kHz) for 60 min then added to the reaction mixture and sonicated (40 kHz) further for 1 h before the reaction started. After the reaction reached room temperature (ca. 25 °C), the pH was adjusted to 3 or 5 using 32 % HCl and stirred overnight.

Metals Boiled Method (HA Method)

In this method, the metal precursors were refluxed for 1 h in EG then the carbon black was added either as is or as a slurry then boiled for a further 3 h where after the pH was adjusted to 3 or 5 again and stirred overnight.

Physical and Electrochemical Characterisations

X-Ray Diffraction (XRD)

X-ray diffractograms of the as-prepared Pt–Sn/C catalyst were obtained on a Bruker AXS D8 Advanced operating with a copper tube with Cu–$K\alpha$ (λ=1.5406 Å) generated at 40 kV and 40 mA. Scans were performed at 0.05° min^{-1} for 2θ values between 10° and 90°. The Debye–Scherrer equation was used as shown in Eq. (1) to estimate the crystal size from the XRD data. For this purpose, the (2 0 0) peak of the Pt*fcc* structure around 2θ=70° was selected to do this, as well as to calculate the lattice parameter (a_{fcc}) values for all the Pt–Sn/C catalyst shown in Eq. (2) [22, 23].

$$d = \frac{0.9\lambda}{\beta \cos\theta} \qquad (1)$$

Where d is the crystal size, 0.9 is the shape factor, λ is the X-ray wavelength, β is the peak width at half peak height and θ is the angle of reflection.

$$a_{fcc} = \frac{\sqrt{2}\lambda_{K\alpha 1}}{\sin\theta} \qquad (2)$$

High-Resolution Transmission Electron Microscopy (HR-TEM)

Visual inspection and analyses of the commercial and produced catalyst nanoparticles were performed using a HR-TEM Technai G2 F20 X-Twin MAT operating at 200 kV. The samples were prepared as follows: a spatula tip of the sample was suspended in ethanol. The mixture was then sonicated (ultrasonic bath, 40 kHz) for approximately 30 min to ensure efficient dispersion. A micropipette was then used to extract some of the sample from the solution which was placed on a S147-4 holey carbon film or 400-mesh copper grids. The copper grid was then left to dry in air. The sample was then placed in the sample tray of the microscope for analysis. The average particle size was calculated using ca. 150 particles. EDX analyses were also determined by HR-TEM.

Electrochemical Characterisations

The performance of Pt–Sn/C catalysts were compared to commercial Pt/C (20 wt.%, HiSPEC™ 3000) catalyst for the MOR and ORR evaluated preliminarily with a half-cell configuration based on the linear sweep voltammetry (LSV) measurements. Then 10 mg of catalysts, 100 µl of Nafion® solution (5 wt.%, Aldrich) and 1.9 ml of water were mixed ultrasonically for 30 min (ultrasonic bath, 40 kHz). A known volume of the catalyst ink was then transferred via a syringe onto a freshly polished (mirror finish) Glassy Carbon (GC) electrode (5 mm in diameter, A_g =0.196 cm^2) to give the desired Pt loading of 30 μg_{Pt} cm^{-2}, which was kept constant for all the electrodes. After the solvents were evaporated in a vacuum oven at 30 °C, the prepared electrode served as the working electrode. Electrochemical measurements were performed using an Autolab PGSTAT 30 potentiostat/galvanostat and a conventional three-electrode electrochemical cell. A platinum foil and Ag/AgCl (3 M KCl) electrodes served as the counter and the reference electrodes, respectively. The electrolyte used for the half-cell measurements was either 0.5 M H_2SO_4 or 0.5 M methanol+0.5 M H_2SO_4. Before electrochemical testing commenced, the electrodes were cycled 25 times at a scan rate of 20 mV s^{-1} between −0.2 and +0.8 V vs. Ag/AgCl until reproducible cyclic voltammograms (CVs) were obtained in views of removing any impurities. The electrochemical activity for the ORR was measured using the

rotating disc electrode (RDE) method. For this purpose, a linear sweep potential of 5 mV s^{-1} from 0 V to +0.8 V vs. Ag/AgCl was applied on the working electrode in an oxygen saturated 0.5 M sulphuric acid solution at various rotating speeds of 500–2,500 rpm. A calculated amount of catalyst ink was dropped onto a GC electrode (5 mm in diameter; A_g = 0.196 cm^2) to achieve the same loading for all the electrodes. High-purity nitrogen (N_2) and oxygen (O_2) were used for de-aeration and oxygenation of the solutions, respectively. For the MOR experiments, the CV scans were carried out in the potential range of −0.2 V to +1.0 V vs. Ag/AgCl at a scan rate of 20 mV s^{-1}. Unless otherwise stated, all half-cell tests were performed at room temperature. During the electrochemical measurements, a blanket of oxygen or nitrogen was maintained above the surface of the solution. The raw RDE data was corrected for background currents by subtracting data recorded in N_2 purged electrolyte over the same potential range, and corrections were applied to compensate for ohmic resistance between the working and the reference electrode, determined by electro-chemical impedance spectroscopy at 10 kHz. All potentials were measured vs. Ag/AgCl (3 M KCl).

Inductively Coupled Plasma–Atomic Emission Spectroscopy (ICP–AES)

For the determination of metal loadings, 40–50 mg of all the catalysts was digested in aqua regia and diluted with ultrapure water to a total of 50 ml. After filtration of the residual carbon black support, the samples were analysed by ICP–AES [Thermo ICap 6300, Pt lamp (λ=214.423 nm) and Sn lamp (λ=284.009 nm)]. NIST traceable certified standards were used for calibration purposes.

Results and Discussions

Characterisation of Pt–Sn/C

Figure 1 shows the XRD pattern of the as-prepared Pt–Sn/C and commercial 20 % Pt/C catalysts. All diffractograms show the faced centred cubic (*fcc*) structure of crystalline Pt.

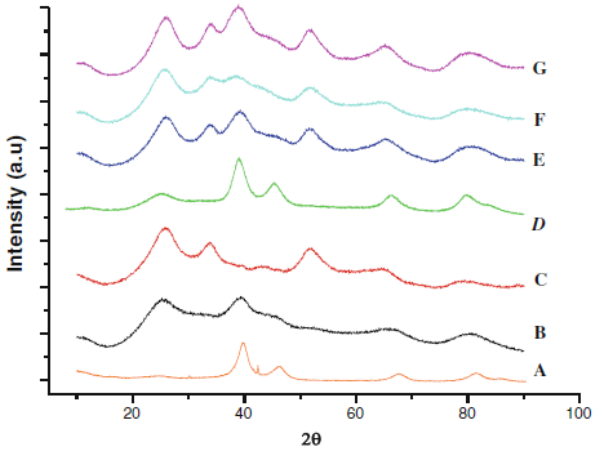

Fig. 1 XRD patterns of **a** 20 % Pt/C, **b** Pt–Sn/C (Slurry pH5), **c** Pt–Sn/C (Slurry pH3), **d** Pt–Sn/C (HA Slurry pH3), **e** Pt–Sn/C (STD), **f** Pt–Sn/C (HA Slurry pH5) and **g** Pt–Sn/C (STD pH3)

The diffraction peak at 26° is attributed to the (0 0 2) plane of the hexagonal phase of Vulcan XC-72 carbon. For the as-prepared Pt–Sn/C catalyst, the diffraction peaks at around 39°, 44°, 66° and 79° correspond to the Pt (1 1 1), (2 0 0), (2 2 0) and (3 1 1) planes, respectively. Compared with the 20 % Pt/C catalyst, the 2θ values shift to slightly lower values confirming that the alloying process of Pt with Sn occurred since Sn enters *fcc* lattice of Pt [19, 23]. In addition, the low intensity peaks around 34° and 52°, respectively, could be attributed to that of the SnO_2 (1 0 1) and SnO_2 (2 1 1) diffraction peaks. The intensity of the SnO_2 phase differs from all the catalysts prepared and the Pt–Sn/C HA Slurry pH3 catalyst exhibited the lowest SnO_2 phase intensity. It is known that SnO_2 dissolves in sulphuric acid so it is suspected that the amount of SnO_2 present in the catalyst is related to the amount of hydrochloric acid added to achieve the desired pH which could possibly play a role in the catalyst methanol-tolerant capabilities [11]. The intensity and broad peak shape point to a relatively close Pt–Pt distance, and thus very small particle sizes are expected. The crystallite sizes calculated from XRD using the Debye–Scherrer equation (Eq. 1) are listed in Table 1 as well as the values of the lattice parameters [23].

Figure 2 depicts the TEM images of three different Pt–Sn/C catalysts synthesised by the modified polyol method. All the images illustrate that the nanoparticles are uniformly dispersed on the surface of the carbon support. The average particle sizes for the catalysts are given in Table 1. Most of the nanoparticles are (1) spherical in shape without evident agglomeration mainly due to the absence of heat treatment of the catalyst and (2) have a narrow particle size distribution. For Pt–Sn/C HA Slurry pH3 samples, most of the particles are in the range of 2.0–3.5 nm with an average particle size of ca. 2.5 nm with a very narrow particle size distribution. Following the procedure to prepare Pt–Sn/C nanoparticles as described by Jeyabharathi et al. [19], the synthesised catalysts showed very poor ORR ability for very low metal loadings. After increasing the temperature, stirring the reaction mixture overnight and ultrasonicating (40 kHz) for an hour, an immediate improvement was observed on the catalyst performance when these changes were implemented into the experimental procedure. Also, the initial change of the pH at the start of the reaction was performed as it plays an important role in controlling the growth and size of the nanoparticles that are formed [24]. Studies performed by Zhao and co-workers [25] describe the effect and mechanism of the polyol method in more detail as to why changing the pH to above 12 is important in the initial stage of the reaction. By using concentrated HCl as the sedimentation promoter, the metal loading increased, the formation of smaller particles as well as a narrower particle size distribution was observed when the pH was dropped and the solution was stirred overnight. This finding also confirmed the work undertaken by Oh et al. who explained this phenomenon, using the zeta potential method for their Pt/C system [26]. After complete reduction of the metal precursors, the nanoparticles were suspended in solution by the glycolate anions which acted as a chelating agent. With the addition of the sedimentation promoter, the glycolate anion concentration was reduced and therefore nanoparticles suspended in solution were freed up leading to metal particles available for deposition onto the carbon support [24–26].

Table 1 Values of lattice parameters and particle size for the as-prepared Pt–Sn/C catalysts

Catalyst	$Pt_{75}Sn_{25}$ phase Lattice parameter (nm)	Crystallite size XRD	Particle size TEM	Sn loading (wt.%)	Pt loading (wt.%)
20 % Pt/C	–	–	–		20.43
Pt–Sn/C (STD)	0.3927	4.2	4.8±0.7	7.32	10.36
Pt–Sn/C (STD pH3)	0.3929	3.8	4.1±0.2	6.24	15.85
Pt–Sn/C (HA Slurry pH3)	0.3931	2.3	2.5±0.3	6.75	19.21
Pt–Sn/C (HA Slurry pH5)	0.3933	2.9	3.1±0.3	7.81	13.33
Pt–Sn/C (Slurry pH3)	0.3926	3.2	3.4±0.3	8.03	18.54
Pt–Sn/C (Slurry pH5)	0.3928	3.5	3.9±0.6	7.52	14.06

Lattice parameter of Pt=0.3923 nm

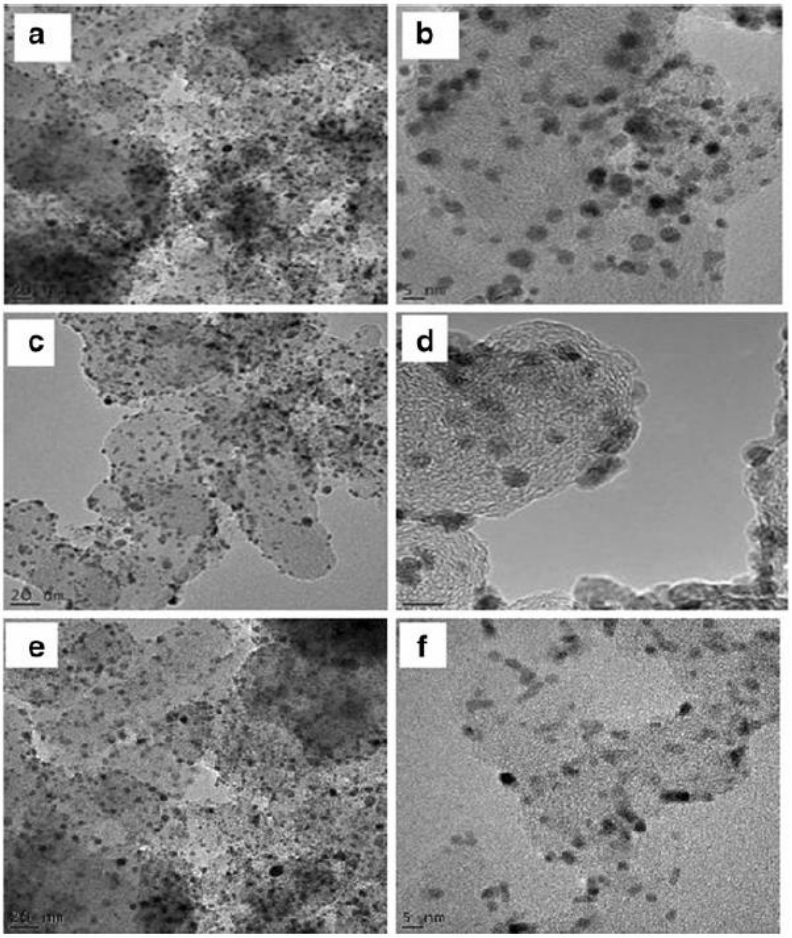

Fig. 2 HR-TEM images of low and high magnification of the as-prepared Pt–Sn/C catalysts **a–b** Pt–Sn/C (STD), **c–d** Pt–Sn/C (Slurry pH 5) and **e–f** Pt–Sn/C (HA Slurry pH3)

This therefore implies that the deposition of the metals onto the carbon support would be higher at lower pH values for these reaction conditions. This is clearly evident in the results from the modified method where the pH was adjusted to 3 (Fig. 2f). The compositions of the Pt–Sn/C catalyst were evaluated by EDX analysis. Figure 3 shows the typical EDX spectra. It was found that there were no foreign elements apart from Pt, Sn, C and Cu (due to the grid). In our study, EDX confirms the presence of Pt and Sn in all the catalysts prepared; furthermore, it was also observed that adding the carbon in a slurry form and ultrasonicating

the samples do play an important role in the particle size and overall particle distribution of the nanoparticles on the carbon support.

Electrochemical Analysis Pt–Sn/C Catalyst

Figure 4 shows the cyclic voltammograms of Pt/C and Pt– Sn/C catalysts in 0.5 M sulphuric acid at a scan rate of 20 mV s^{-1} and in the potential range of Ag/AgCl. The cyclic voltammograms of the Pt/C catalysts are typical of unalloyed Pt with clearly resolved hydrogen adsorption/desorption peaks at −0.2 to +0.1 V vs. Ag/AgCl.

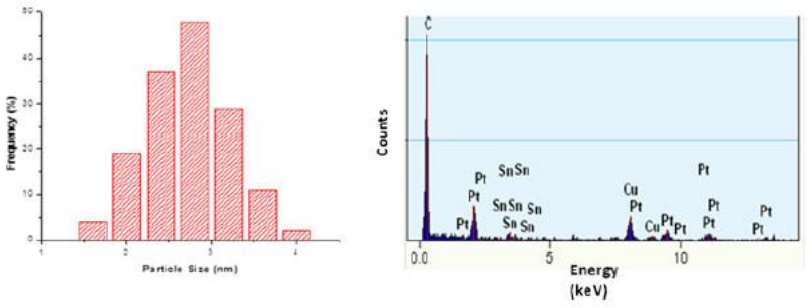

Fig. 3 Particle size distribution and EDX spectrum of Pt–Sn/C (HA Slurry pH3) catalyst

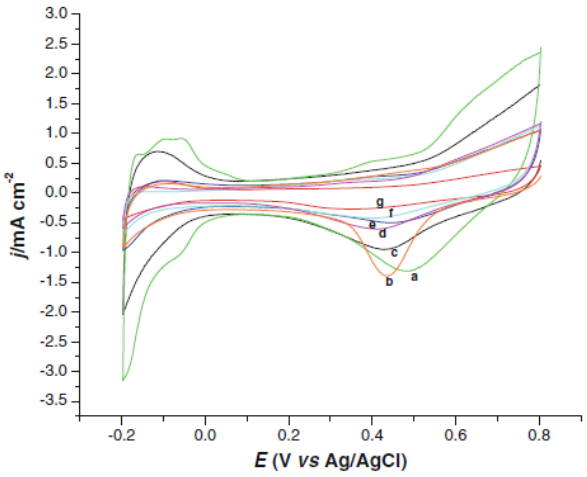

Fig. 4 Cyclic voltammograms obtained for a Pt–Sn/C catalyst and compared to that of a commercial Pt/C catalyst in a 0.5 M H_2SO_4 solution; scan rate of 20 mV s^{-1} and at room temperature

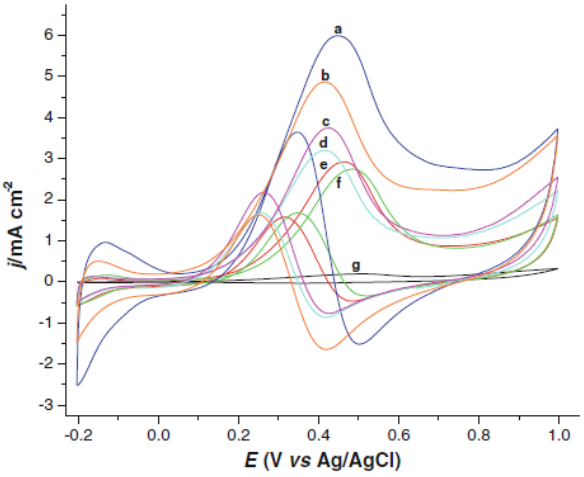

Fig. 6 Cyclic voltammograms of methanol tolerance obtained on a Pt–Sn/C electrode after adding 50 µl methanol and compared with that of commercial Pt/C in 0.5 M H_2SO_4 solution; scan rate 20 mV s^{-1}

Only the commercial Pt/C and Pt–Sn/C STD pH3 catalysts showed well-defined hydrogen desorption/adsorption peaks (of various amplitudes) implying a low degree of alloying with Sn and the presence of a high portion of tin oxide phase [27]. By comparing the CVs obtained for pure Pt and bi-metallic Pt–Sn, it was observed that the peak potential corresponding to the reduction of platinum oxide (PtO) has shifted slightly towards lower potentials (ΔE= −50 mV). This can be possibly explained by either the strengthening of the Pt–O bond or by the effect of tin on the reaction kinetics and/or to the formation of an alloy [28]. From the CVs, it is evident that the incorporation of Sn seems to 'block' some of the Pt active sites which in turn resulted that no distinct hydrogen adsorption/desorption region was

observed for Pt–Sn/C in comparison with Pt/C. This further confirms the alloying between Pt and Sn [19].

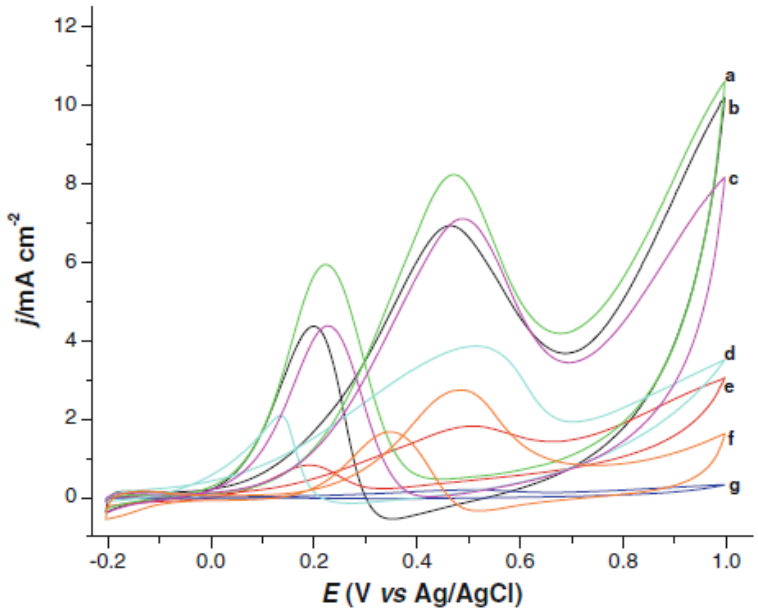

Fig. 5 Cyclic voltammograms of methanol oxidation obtained on a Pt –Sn/C electrode and compared with that of Pt/C in 0.5 M H_2SO_4 solution containing 0.5 M methanol; scan rate 20 mV s^{-1}

Methanol Oxidation

In order to evaluate the as-prepared Pt–Sn/C catalyst for MOR, all data were compared to commercial 20 % Pt/C in 0.5 M sulphuric acid+0.5 M methanol solutions as shown in Fig. 5. The figure shows that the methanol oxidation current of +7.08 mA at a potential of +0.48 V vs. Ag/AgCl for Pt– Sn/C HA Slurry pH3 is less than that of the commercial Pt/C which was 8.25 mA at the same potential and for the same Pt loading. It can be observed that all the Pt–Sn/C catalysts showed lower methanol oxidation currents indicating that the Pt–Sn/C system do have methanol-tolerant capabilities. The Pt–Sn/C catalyst synthesised using the STD method for example keeping the pH at 13 shows the lowest oxidation current indicating that adding HCl after the reaction is complete has a detrimental effect on the activity of the catalyst as well as the amount of metal deposited onto the carbon support. ICP studies confirmed this finding as the STD method showed the lowest percentage amount of Pt deposited on the carbon support and the lowest MOR response for Pt–Sn/C STD catalyst was observed.

Data in Fig. 6 were obtained after adding aliquots of methanol (10–1,000 µl) to the electrochemical cell containing 50 ml of 0.5 M H_2SO_4. The amount of methanol was increased with each scan to investigate the ability of the catalyst to show resistance towards methanol if small amount of methanol permeates through the membrane.

Table 2 Parameters derived from ORR and MOR data of the as-prepared Pt–Sn/C catalysts

Catalyst	SA at 0.65 V ($\mu A\ cm^{-2}_{Pt}$)	MA at 0.65 V ($A\ mg^{-1}_{Pt}$)	Tafel slope ($mV\ dec^{-1}$)	MOR current ($mA\ cm^{-2}$) after 50 µl at 0.45 V
20 % Pt/C	283±44	0.24±0.03	−59 −119	5.98
Pt–Sn/C (STD)	98±12	0.09±0.01	−80 −196	0.19
Pt–Sn/C (STD pH3)	135±26	0.11±0.02	−71 −140	2.69
Pt–Sn/C (HA Slurry pH3)	304±35	0.27±0.02	−62 −122	4.81
Pt–Sn/C (HA SlurypH5)	204±18	0.10±0.04	−70 −178	3.14
Pt–Sn/C (Slurry pH3)	237±29	0.19±0.01	−77 −160	3.73
Pt–Sn/C (Slurry pH5)	179±51	0.14±0.01	−73 −185	2.93

The shape of the CV for the commercial Pt/C changed immediately at +450 mV vs. Ag/AgCl as soon as the methanol (10 µl) was added to the solution. In the case for the as-prepared Pt–Sn/C catalyst, the activity towards methanol oxidation was only observed after adding 30 µl of methanol addition. For the Pt–Sn/C STD catalyst samples even after adding 500 µl methanol, no methanol oxidation peaks were observed at +450 mV vs. Ag/AgCl. The results after adding 50 µl methanol to all the Pt–Sn/C catalysts are shown in Table 2. All of the synthesised Pt–Sn/C showed a lower methanol oxidation current response at ca. +450 mV vs. Ag/AgCl when compared to the methanol oxidation current for Pt/C for the same amount of methanol added. The Pt– Sn/C STD catalyst performed the best of the as-prepared catalyst delivering the lowest current after adding 50 µl methanol to the electrolyte.

Oxygen Reduction Kinetics of Pt–Sn/C Catalysts

To obtain kinetic information for the Pt–Sn/C catalysts, rotating disc electrode (RDE) experiments were performed under steady-state conditions. Figure 7 show the ORR curves for the as-prepared Pt–Sn/C catalysts at a rotation speed of 1,500 rpm in oxygen saturated 0.5 M H_2SO_4 solution at room temperature in the potential region of 0 V to +0.80 V vs. Ag/AgCl at a scan rate of 5 mV s^{-1}. In the diffusion-limited region, i.e. 0 V to +0.45 V vs. Ag/AgCl, the total current J of the ORR comprises of the diffusing and kinetic part as expressed by the Koutecky–Levich (K–L) equation (Eq. 3) [29]:

$$\frac{1}{j}=\frac{1}{j_k}+\frac{1}{0.62nFD_0^{2/3}\omega^{1/2}\nu^{-1/6}C_0}=\frac{1}{j_k}+\frac{1}{B\sqrt{\omega}} \qquad (3)$$

where j is the disk electrode current density and j_k is the kinetic current density, B is the Levich slope, n is the number of electrons involved in the ORR per oxygen molecule, C is the saturation concentration for oxygen in the electrolyte (1.26×10^{-3} mol L^{-1}), D is the diffusion coefficient of oxygen (1.93×10^{-5} cm^2 s^{-1}), υ is the kinematic viscosity of the solution (1.009×10^{-2} cm^2 s^{-1}) and ω is the rotation speed (rpm).

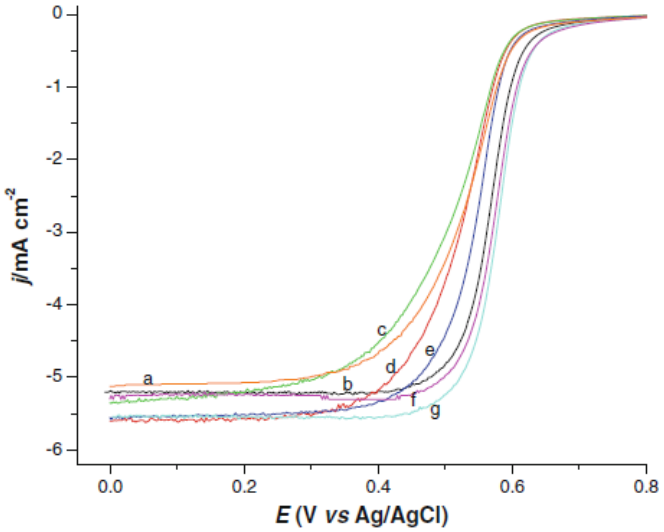

Fig. 7 Polarisation curves obtained with a RDE for O_2 reduction on a Pt–Sn/C electrode and compared with that of commercial Pt/C in 0.5 M H_2SO_4 solution at 1,500 rpm; scan rate 5 mV s^{-1}. **a** Pt–Sn/C (Slurry pH5), **b** Pt–Sn/C (Slurry pH 3), **c** Pt–Sn/C (STD), **d** Pt–Sn/C (HA Slurry pH5), **e** Pt–Sn/C (STD pH3), **f** 20 % Pt/C and **g** Pt–Sn/C (HA Slurry pH3)

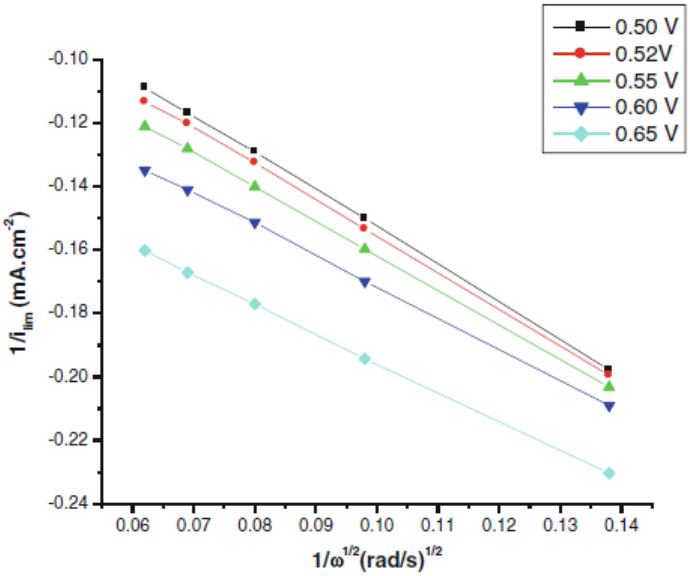

Fig. 8 Koutecky–Levich plots for Pt–Sn/C HA Slurry pH 3 (data generated from Fig. 7)

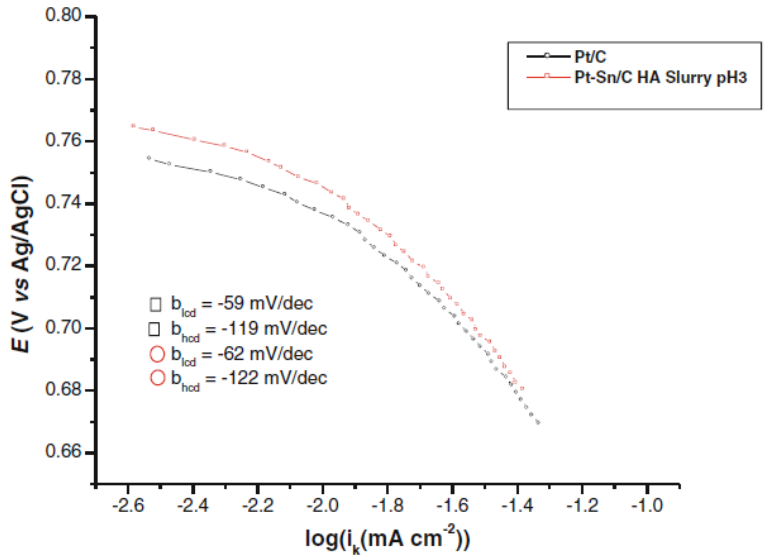

Fig. 9 ORR mass-transfer corrected Tafel polarisation curves for Pt/C and Pt–Sn/C catalysts, at room temperature, a rotation speed of 1,500 rpm, a scan rate of 5 mV s^{-1} in oxygen saturated 0.5 M H_2SO_4 solution

The number of electrons involved in the ORR was calculated using the K–L equation, which relates to the current density i to the rotation speed of the GC electrode, ω. A plot of j^{-1} *vs.* $\omega^{-1/2}$ gave parallel straight lines at various potentials in the range of +0.5 V to +0.7 V vs. Ag/AgCl in the mixed diffusion controlled region. The K–L plots of all the Pt– Sn/C catalyst showed (Fig. 8) linearity confirming that the oxygen reduction reaction follows first-order kinetics.

Further kinetic information regarding the electron transfer reaction was gained when the Pt–Sn/C and Pt/C catalysts were compared as shown in Fig. 9. The figure shows mass-transfer Tafel polarisation curves in the range of $\pm 0.65 < E < \pm 0.77$ V vs. Ag/AgCl for the commercial Pt/C and the as-prepared Pt–Sn/C which are summarised in Table 2. The data were obtained at room temperature in 0.5 M H_2SO_4 saturated with oxygen at 1,500 rpm based on an anodic scan from 0 V to +0.80 V vs. Ag/AgCl at a scan rate of 5 mV s^{-1}. Two Tafel slopes, i.e. ca. −59 and −62 mV dec^{-1} in the low current region and −119 and −122 mV dec^{-1} for the high current region were found for Pt/C and Pt–Sn/C HA Slurry pH3, respectively. For the commercial Pt/C, the low and high Tafel slopes were in excellent agreement with values found in the literature [30]. The Tafel slopes of the Pt–Sn/C HA Slurry pH3 were almost the same to that of the commercial Pt/C. This could be explained in terms of the coverage of the electrode surface by adsorbed oxygen which follows a Langmuir isotherm (low coverage) at high overpotential and a Temkin isotherm (high coverage) at lower overpotentials [1, 31, 32].

This implies that the rate-determining step for the ORR is unchanged for both catalyst despite some differences in their electrocatalytic properties [1, 32]. However, Tafel slopes values calculated by ORR for the other Pt–Sn/C catalyst suggest a rather complex reaction mechanism(s). Of all the catalysts synthesised, the Pt–Sn/C HA Slurry pH3 catalyst showed similar catalytic activity towards ORR and gave an indication that the catalytic mechanism for

ORR might be the same as that of Pt/C indicating that the ORR kinetics was not negatively influenced by the addition of tin.

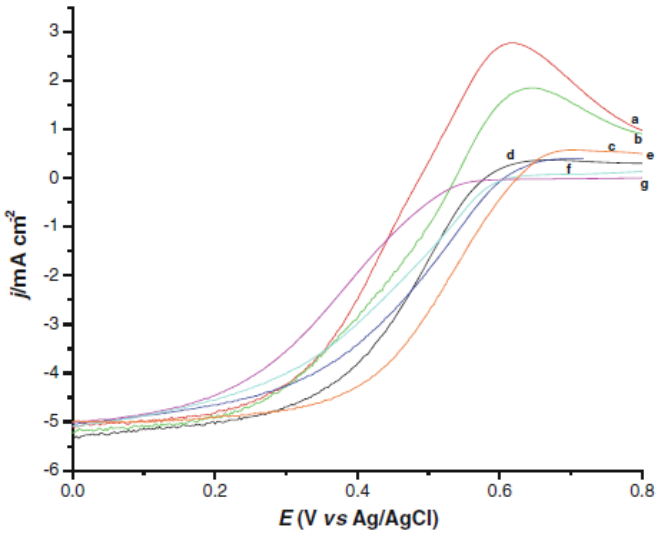

Fig. 10 RDE polarisation curves for Pt/C and Pt–Sn/C catalysts in 0.5 M H_2SO_4+0.5 CH_3OH under oxygen atmosphere at a scan rate of 5 mV s^{-1}, a rotating speed of 1,500 rpm and at room temperature. **a** 20 % Pt/C, **b** Pt–Sn/C (HA Slurry pH3), **c** Pt–Sn/C (Slurry pH3), **d** Pt–Sn/C (STD pH3), **e** Pt–Sn/C (Slurry pH5), **f** Pt–Sn/C (HA Slurry pH 5) and **g** Pt–Sn/C (STD)

Thus in our study, the activity towards ORR was found to be as follows: Pt–Sn/C (HA Slurry pH3)>Pt–Sn/C (Slurry pH3)> Pt–Sn/C (Slurry pH5)>Pt–Sn/C (HA Slurry pH5)> Pt–Sn/C (STD pH3), Pt–Sn/C (STD).

Methanol Tolerance Study

It is known that the crossover of methanol from the anode to the Pt-based cathode can lead to further reduction of cell voltage by ca. ~200–300 mV [19]. Thus, it is highly desirable that the synthesised Pt–Sn/C eletrocatalysts should show a high degree of methanol tolerance for DMFC applications. Figure 10 shows the ORR activity of Pt/C and Pt–Sn/C catalysts in the presence of 0.5 M methanol to study the methanol-tolerant properties of the synthesised Pt–Sn/C. The potential was scanned from 0 V to +0.8 V vs. Ag/AgCl at a scan rate of 5 mV s^{-1} under an oxygen atmosphere. As compared to the ORR in pure H_2SO_4 solution (Fig. 7), the Pt/C and Pt–Sn/C catalysts exhibited an anodic current at ca. +600 mV vs. Ag/AgCl corresponding to the oxidation of methanol on the catalysts. All the catalysts for the ORR showed an increase in overpotential (ca. +20 to +200 mV) in the presence of methanol. This increase may be due to the simultaneous oxidation of methanol and oxygen reduction on the surface of the catalyst. The increase in overpotential for Pt/C was also found to be the highest when compared to the synthesised Pt–Sn/C catalyst, and such a high mixed potential at the cathode could negatively affect the performance of the DFMC. It is thus clear from

Fig. 10 that the different Pt–Sn/C catalysts are less affected by the presence of methanol in solution than Pt/C under similar conditions.

This finding implies that the Pt–Sn/C catalyst system might be a potentially good active cathodic catalyst for applications in DMFCs with methanol-tolerant capabilities. The ability of the catalyst to show methanol-tolerant behaviour can be described by the so-called geometric 'ensemble' effect [4, 14, 20]. The second metal or metal oxides (Sn, SnO_2) atoms around the Pt active sites may block methanol oxidation on the Pt sites due to the ensemble effect. Therefore, methanol oxidation on the binary system can be suppressed. On the other hand, only two adjacent Pt sites are required for the dissociative chemisorption of oxygen and Pt is less affected by the presence of Sn or SnO_2. The composition of the as-prepared Pt–Sn/C bi-metallic catalyst, which is 3:1, results in a low activity towards methanol oxidation and therefore a high methanol tolerance towards the ORR [20]. In our investigation, the order of electrocatalytic resistance towards methanol is as follows: Pt–Sn/C (STD)> Pt–Sn/C (STD pH3)> Pt–Sn/C (Slurry pH5)> Pt–Sn/C (HA Slurry pH5)> Pt–Sn/C (Slurry pH3)> Pt–Sn/C (HA Slurry pH3).

Conclusions

Pt–Sn/C catalysts were synthesised using a modified polyol reduction method using HCl as sedimentation promoter. The average particle size distributions were found to be in the range of 2.5–5.6 nm for the various as-prepared catalysts from HR-TEM results. 2θ values shifted to lower angle values in XRD confirming the alloying of Sn with Pt. Of the six catalyst samples studied, Pt–Sn/C (STD) and Pt– Sn/C (HA Slurry pH3) showed the best performance towards MOR resistance and ORR, respectively. The Tafel slopes of Pt–Sn/C HA Slurry pH3 catalyst samples suggest that the ORR mechanism is similar to that of the commercial Pt/C. Adding HCl and ultrasonicating the samples before the reaction commences plays an important role towards the activity of the catalyst.

Acknowledgements

The authors would like to acknowledge financial support from the National Research Foundation (NRF), Energy Supply Commission (ESKOM) and the University of the Western Cape (UWC).

References

1. G. Pérez, E. Pastor, C.F. Zinola, Int. J. Hydrogen Energy. 34, 9523 (2009)
2. E. Antolini, T. Lopes, E.R. Gonzalez, J. Alloys Compd. 461, 253 (2008)
3. K. Ramya, K.S. Dhathathreyan, J. Electroanal. Chem. 542, 109 (2003)
4. C. Lamy, A. Lima, V. Le Rhun, C. Coutanceau, J.M. Leger, J. Power Sources. 105, 283 (2002)
5. A.K. Shuka, R.K. Raman, Annu. Rev. Mater. Res. 33, 155 (2003)
6. V. Baglio, A. Stassi, A. Di Blasi, C. D'Urso, V. Antonucci, A.S. Arico, Electrochim. Acta. 53, 1360 (2007)
7. V. Stamenkovic, T.J. Schmidt, P.N. Ross, N.M. Markovic, J. Phys. Chem. B. 106, 11970 (2002)
8. R.Z. Jiang, D.Y. Chu, J. Electrochem. Soc. 147(4605) (2000)
9. A. El Hourch, C. Coutanceau, J.M. Léger, C. Lamy, Electroanal. Chem. 429, 117 (1997)
10. P. Convert, C. Coutanceau, F. Gloaguen, C. Lamy, J. Appl. Electrochem. 31, 945 (2001)
11. N. Alonso-Vante, P. Bogdanoff, H. Tributsch, J. Catal. 190, 240 (2000)
12. M. Bron, P. Bogdanoff, S. Fiechter, M. Hilgendorff, J. Electroanal. Chem. 517, 85 (2001)
13. F. Maillard, M. Martin, F. Gloaguen, J.M. Léger, Electrochim. Acta. 47, 3431 (2002)
14. E. Antolini, E.R. Gonzalez, Catal. Today. 160, 28 (2011)
15. S. Mukerjee, J. McBreen, J. Electrochem. Soc. 146, 600 (1999)
16. G. Stalnionis, L. Tamasauskaite-Tamasiunaite, V. Pautieniene, Z. Jusys, J. Solid State Electrochem. 8, 892 (2004)
17. H. Gasteiger, N. Markovic, P. Ross, E.J. Cairns, Electrochim. Acta. 39(1825) (1994)